Solar Phys
DOI 10.1007/s11207-015-0694-z

Remote-Sensing of Solar Wind Speeds from IPS Observations at 140 and 327 MHz Using MEXART and STEL

J.C. Mejia-Ambriz[1,2] · B.V. Jackson[1] · J.A. Gonzalez-Esparza[2] · A. Buffington[1] · M. Tokumaru[3] · E. Aguilar-Rodriguez[4]

Received: 19 February 2014 / Accepted: 30 April 2015

Abstract Interplanetary scintillation (IPS) is used to probe solar wind speeds in the inner heliosphere by applying either of two generalized data-analysis techniques: model fitting to power spectra (MFPS) from a single station, or cross-correlation functions (CCF) produced by cross-correlating two simultaneous IPS time series from separate stations. The *MEXican Array Radio Telescope* (MEXART), observing at 140 MHz, is starting to use an MFPS technique. Here we report the first successful solar wind speed determinations with IPS observations by MEXART. Three stations of the Solar-Terrestrial Environment Laboratory (STEL), observing at 327 MHz, use a CCF, and an MFPS technique is also used at one of these sites. We here analyze data from MEXART and from one antenna of STEL to obtain

Radio Heliophysics: Science and Forecasting
Guest Editors: Mario M. Bisi, Bernard V. Jackson, and J. Americo Gonzalez-Esparza

✉ J.C. Mejia-Ambriz
jcmejia@geofisica.unam.mx

B.V. Jackson
bvjackson@ucsd.edu

J.A. Gonzalez-Esparza
americo@geofisica.unam.mx

A. Buffington
abuffington@ucsd.edu

M. Tokumaru
tokumaru@stelab.nagoya-u.ac.jp

E. Aguilar-Rodriguez
ernesto@geofisica.unam.mx

[1] Center for Astrophysics and Space Sciences, University of California, San Diego, 9500 Gilman Drive, La Jolla, CA 92093-0424, USA

[2] SCiESMEX, Instituto de Geofisica, Unidad Michoacan, Universidad Nacional Autonoma de Mexico, Morelia, Michoacan, 58190, Mexico

[3] Solar-Terrestrial Environment Laboratory, Nagoya University, Nagoya, Japan

[4] Instituto de Geofisica, Unidad Michoacan, Universidad Nacional Autonoma de Mexico, antigua carretera a Patzcuaro 8701 Ex-Hda, San Jose de la Huerta Morelia, Michoacan, 58089, Mexico

Published online: 22 May 2015

solar wind speeds using an MFPS technique from a single station. The IPS observations were carried out with radio source 3C48 during Solar Cycle 24. The MFPS method we describe here is tested by comparing its obtained speeds with those from the STEL CCF technique. We find that the speeds from the two techniques generally agree within the estimated errors.

Keywords Radio scintillation · Solar wind, disturbances · Waves, propagation

1. Introduction

Radio waves emitted from compact (angular width $\lesssim 1$ arcsec) radio sources are scattered by small-scale (10^1 to 10^3 km) electron-density fluctuations in the solar wind plasma. At Earth, this scattering appears as a radiation pattern that moves along with the solar wind. Since the 1960s (Hewish, Scott, and Wills, 1964; Little and Hewish, 1966; Cohen and Gundermann, 1969), this phenomenon has been observed by radio telescopes as intensity fluctuations in the flux from radio sources, and it is known as interplanetary scintillation (IPS). IPS is widely used as a powerful remote-sensing tool for exploring solar wind properties, such as density, turbulence, and velocity over the whole inner heliosphere (*e.g.*, Swarup *et al.*, 1971; Readhead, Kemp, and Hewish, 1978; Scott, Rickett, and Armstrong, 1983; Coles *et al.*, 1995; Jackson *et al.*, 1998; Bisi *et al.*, 2010; Tappin and Howard, 2010; Kojima *et al.*, 2013). Figure 1 shows the IPS phenomenon and the methods we used to measure solar wind speeds. Here the elongation angle ϵ is formed by the Sun–Earth line and the line of sight (LOS) to the source. Most of the scattering along the LOS is close to the region of closest approach to the Sun, the center of this region is identified with the 'P-point' (see Figure 1), located at heliocentric distance $\sin(\epsilon)$ in AU. The LOS can be outside the ecliptic plane, thus placing P at different heliocentric latitudes.

To obtain solar wind speeds from the observed time series of intensity fluctuations, there exist two techniques: model fitting to power spectra (MFPS) of observations with a single

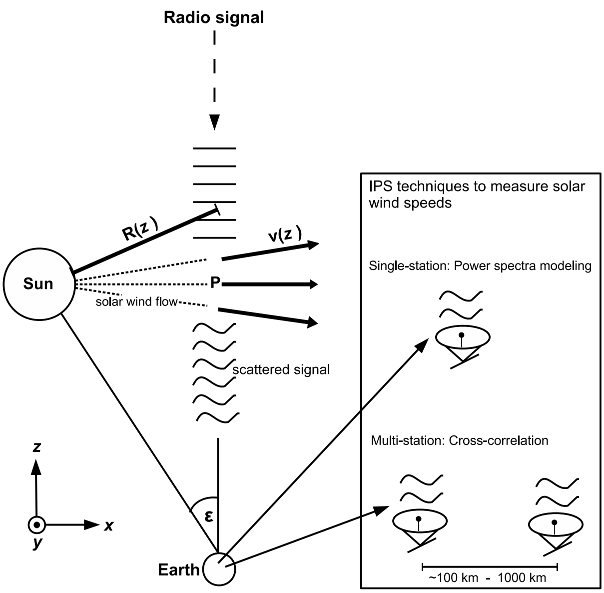

Figure 1 IPS is a tool for measuring solar wind speeds in the inner heliosphere using one or more radio stations. The contribution of solar wind fluctuations along the LOS diminishes as R^{-4}, so the resulting spectrum is dominated near the P-point. The origin of the coordinates here is at point P and the signal from the distant source travels to Earth as shown along the z axis. T is the distance from Earth to the P-point and $V_x(z)$ is the velocity component in the x direction on the LOS.

Table 1 Technical characteristics of the radio telescopes: MEXART and SWIFT.

	MEXART	SWIFT
Type of antenna	Plane array, 4 096 full-wavelength dipoles[a]	2 cylindrical parabolas, 384 half-wavelength dipoles
Observing freq (MHz)	139.65	327
Bandwidth (MHz)	2	10
Location	19°48′N, 101°41′W	34°50′N, 137°23′E
Beam width E–W	1°	1.3°
Collection area (m^2)	9 800 (for full array)	3 344
Integration time τ (ms)	47	20
Sampling rate (Hz)	50	50

[a]Observations in this work were carried out with 1 024 dipoles in 2009 (quarter of the total) and 2 048 dipoles (half of the total) in 2012 and 2013.

station, and cross-correlation functions (CCF) of data produced by two or more stations. Single-station speeds are determined by using the technique first tested by Scott, Coles, and Bourgois (1983) and later employed by Manoharan and Ananthakrishnan (1990). They applied MFPS to IPS flux fluctuations. The model is constructed by solving an equation for a wave propagating through a thin dispersive layer of plasma in the weak scattering region (Salpeter, 1967; Bastian, 2000), then integrating the contribution of layers along the LOS, and expressing the result as a theoretical power spectrum that depends on several physical parameters, including the observing frequency, solar wind velocity, and the apparent structure of the radio source. The multi-station technique, first developed by Hewish, Dennison, and Pilkington (1966), uses two or more observing sites that are located far enough apart to measure the timing difference of the scintillation pattern from one site to another. Typical separations are about 100 km, although studies have obtained speeds by using extremely long baselines with separations of 900 km (Rao *et al.*, 1996) and 2 000 km (Breen *et al.*, 2006). The basic principle estimates the radiation pattern delay between the stations, obtained by the time lag for the maximum of the CCF of the observed intensity fluctuations (Vitkevich and Vlasov, 1970; Coles and Kaufman, 1978; Fallows *et al.*, 2006; Kojima *et al.*, 2013). This way, a drift speed of the radiation pattern is derived.

The net IPS observations are a result of the distribution of speeds along the LOS, but these are dominated by the contributions near the P-point. Some multi-site surveys from CCF show that it is possible to distinguish more than one distinct speed along the LOS, *e.g.*, Grall *et al.* (1996) and Moran *et al.* (2000) showed slow and fast streams; later studies showed signatures of three streams in the CCF (*e.g.*, Breen *et al.*, 2008; Bisi *et al.*, 2010). We determined the magnitude of a component of the solar wind velocity, the speed, from integrating the distribution of velocity components along the LOS. These components are perpendicular to the LOS and directed toward the solar wind outflow (the x direction in Figure 1).

Two newly developed instruments are compared here; both are dedicated to full-time IPS studies: The *MEXican Array Radio Telescope* (MEXART) at 140 MHz (Gonzalez-Esparza *et al.*, 2004; Mejia-Ambriz *et al.*, 2010), and the *Solar Wind Imaging Facility* (SWIFT; Tokumaru *et al.*, 2011) of the Solar-Terrestrial Environment Laboratory (STEL) at 327 MHz (see the general characteristics of the arrays in Table 1). In 2009, MEXART saw its first IPS light (Mejia-Ambriz *et al.*, 2010), and now it is adopting the MFPS technique to determine solar wind speeds. MEXART currently provides the only IPS observations in the Americas, and thus has a unique longitudinal location to monitor compact sources from Earth's western hemisphere; thus MEXART complements STEL observations (and other radio systems) to monitor space weather during times of day when these other systems cannot view a particular selection of sources near the Sun. Other systems include the *Ooty Radio Telescope* (ORT) of India, the *LOw Frequency ARray* (LOFAR) in the Netherlands and across central and western Europe, the *Big Scanning Array* (BSA) in Russia, the *European Incoherent SCATter* (EISCAT) radar in northern Scandinavia, and the *Korean IPS Array* in South Korea. Up to now, MEXART has operated with a fraction of the total array (see Table 1), which currently limits the number of observed sources. However, the IPS observations reported here have good enough signal-to-noise ratios to extract reliable solar wind speed information from the power spectra. The STEL IPS system consists of four antennas (although only three are now used) for the CCF analysis; SWIFT, one of the three antennas for CCF analysis, is the most sensitive station of STEL and thus provides more LOSs each day, enabling the best resolution of the systems studied to reconstruct the dynamics of the solar wind using IPS tomography programs (*e.g.*, Kojima *et al.*, 1998; Jackson *et al.*, 2010, 2013).

We report here the first solar wind speed measurements using observations at 140 MHz. We applied the MFPS technique to IPS observations from both MEXART and SWIFT. Solar wind speeds obtained from MFPS with SWIFT agree with speeds from CCF, using three stations of STEL, one of which is SWIFT. Solar wind speeds using one site at STEL are especially useful when data are available from only one antenna; application of an MFPS technique for the STEL system is also separately under study (Tokumaru *et al.*, 2011). The present work provides a calibration of MFPS using data of MEXART and SWIFT. Of particular importance here is our discussion of the resulting accuracy for solar wind speeds with MFPS; the other physical parameters are not treated in detail. Section 2 explains the model of the IPS power spectrum focusing on observations at 140 MHz and 327 MHz. Section 3 presents general characteristics of the arrays, epoch of observations, and important differences of the observations between the two radio telescopes used here. Two tables in this section summarize the MFPS solar wind speed results and associated errors with SWIFT and MEXART and compare them with the CCF results obtained with STEL. Section 4 describes both the process of generating the power spectra of IPS and the methodology used to measure the solar wind speeds by fitting the model to the observed power spectra. Section 5 is an analysis of the principal results. Finally, a summary and conclusions are given in Section 6.

2. The Model for IPS Power Spectra

The model used here from a single station for IPS taken in the weak-scattering regime is the result from integrating physical properties along the LOS. The model can be represented by a theoretical temporal power spectrum $P(f)$, where f is the frequency of scintillation (*e.g.*, Manoharan, 2010). Using a coordinate system (Figure 1) with its z axis along the LOS (the origin of z at the P-point and positive direction toward the source), this is

$$P(f) = C \int_{z=-T}^{2\mathrm{AU}-T} \mathrm{d}z \frac{1}{V_x(z)} \int_{q_y} \mathrm{d}q_y F_\mathrm{d} F_\mathrm{s} \Phi_{N_\mathrm{e}}, \tag{1}$$

where F_d, F_s, and Φ_{N_e} are functions of the spatial wave number (components q_x, q_y) and z. $V_x(z) = 2\pi f / q_x$ is the outflow velocity component perpendicular to z in the plane of Figure 1. The integral along q_y is evaluated over wave numbers of irregularities that scatter the

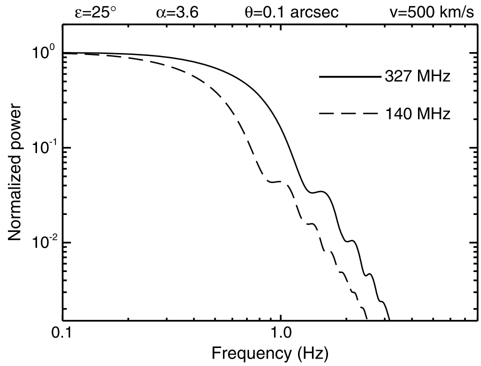

Figure 2 Theoretical IPS power spectra *versus* scintillation frequency for the indicated values and observing frequencies: MEXART (dashed) and STEL (solid curve). Both spectra have equal parameters except for the observing frequency. Curves normalized to unity at 0.1 Hz.

radio waves ($q_y \approx 10^{-3}$ to 10^{-1} km^{-1}). $T = \cos(\epsilon)$ in AU is the distance from Earth to the P-point. $C = (2\pi r_e \lambda)^2$, where r_e is the electron radius and λ is the observing wavelength. Figure 2 shows an example of two solutions of the model.

F_d is the diffractive contribution of the scattered signal given by

$$F_d = 4\sin^2\left(\frac{q^2 z_0 \lambda}{4\pi}\right), \tag{2}$$

and is commonly known as the Fresnel filter, where $q^2 = q_x^2 + q_y^2$ and $z_0 = z + T$.

Assuming a symmetrical-Gaussian brightness distribution for the source, the square modulus of the Fourier transform of this distribution, F_s, is given by

$$F_s = \exp\left[-(q z_0 \theta/2.35)^2\right], \tag{3}$$

which is the visibility function squared, where θ is the angular width at half-maximum diameter of the radio source in radians.

The Fresnel filter and the visibility function block low and high wavenumbers, respectively; the two combined result in a band-pass filter. At the P-point this filter allows fluctuations within the interval $V_x/\sqrt{\pi\lambda T} < f < 0.37 V_x/T\theta$. For the case of Figure 2, $0.8 < f < 2.8$ Hz and $0.5 < f < 2.8$ Hz at 327 and 140 MHz, respectively.

The function Φ_{N_e} is the spectrum of the electron-density fluctuations (ΔN_e). This spectrum depends on the shape of the irregularities, which are usually elongated along magnetic-field lines close-in to the Sun (Grall *et al.*, 1997), and thus can be modeled as ellipses where the ratio of their axes is defined as the axial ratio. Additionally, Φ_{N_e} has a cutoff at a high wave number (q_i) that corresponds to the smallest (or inner scale) size of irregularities contributing to IPS. Assuming an isotropic medium (axial ratio = 1) for large heliocentric distances (Rickett and Coles, 2000) and that the contribution of inner scale of irregularities is insignificant for extended sources (Manoharan, 2010), Φ_{N_e} is simplified as

$$\Phi_{N_e} \propto q^{-\alpha} R^{-\beta}. \tag{4}$$

From IPS observations $\beta \approx 4.0$ (Readhead, 1971; Armstrong and Coles, 1978; Armstrong, Coles, and Rickett, 2000; Kojima *et al.*, 2013) and $\alpha \approx 3.4 \pm 0.6$ (Scott, Coles, and Bourgois, 1983; Scott, Rickett, and Armstrong, 1983; Manoharan and Ananthakrishnan, 1990; Manoharan, Kojima, and Misawa, 1994; Yamauchi *et al.*, 1996; Bastian, 2001). This rapid gradient makes the scattering most sensitive near the P-point. In fact, the scattering results in an amplitude scintillation bias just anti-Earth of the P-point of the LOS from antenna to the source. The limits of integration along the LOS in Equation (1) are enough to obtain nearly all contributions from the medium to the IPS. Therefore, most of the contribution to the power spectra is generated by the scattering from Earth to 2 AU.

The theoretical power spectrum resulting from typical solar wind parameters is flat at low frequencies (Figure 2), then has a sudden drop over the Fresnel knee (near 1 Hz in Figure 2) to the first minimum. The Fresnel-knee region can be defined as $V_x/\sqrt{2\lambda T} < f_{\mathrm{F}} < V_x/\sqrt{\lambda T}$; the Fresnel knee moves to higher scintillation frequency proportional to the square root of the observing frequency, because lower radio-wave observing frequencies are scattered by solar wind irregularities of larger size. Thus when the same IPS source is observed at 140 and 327 MHz under similar solar wind conditions, we expect the Fresnel knee of the observed power spectrum at 327 MHz to be shifted higher by ≈ 1.5 times in spectra frequency relative to the knee at 140 MHz (see Figure 2; also Figure 3 in Section 4). Moreover, since astronomical radio sources often appear smaller when observing at higher frequencies (Janardhan and Alurkar, 1993; Shen *et al.*, 2005), this effect makes the shift even wider. It should be noted that all the above model parameters influence the obtained speeds, therefore errors in these values can lead to incorrect speed estimates. A more detailed investigation of potential systematic errors that are due to this is beyond the scope of this article, but see discussion below just after Equation (5).

3. IPS Observations

Table 1 presents the basic technical characteristics of MEXART and SWIFT. MEXART is composed of 64 East–West rows with 64 dipoles each. SWIFT consists of two cylindrical parabolic reflector antennas (192 half-wavelength dipoles each). These are both transit instruments: when a natural radio source passes through a beam, the flux is recorded within a FWHM during about 4 min for MEXART and 5.25 min for SWIFT. The difference in geographic longitude ($\approx 121^\circ$) introduces time offsets of approximately 8 or 16 h for observations of the same radio source. MEXART commenced the observations of suitably compact astronomical radio sources in 2009 using just one quarter of the final array, and from 2011 to 2013 with half of the array. We used 17 observations of 3C48 by MEXART in April 2009, May 2012, and from February to May 2013. These were made during the epoch of solar minimum (2009) passing through the ascending phase to the maximum (2012 – 2013) of Solar Cycle 24, at elongation angles $22^\circ \leq \epsilon \leq 63^\circ$ (P-point from 0.37 to 0.89 AU) with the P-point located at heliocentric latitudes from $\approx 20^\circ$ to $\approx 60^\circ$; these elongations are within the weak-scattering regime at 140 and 327 MHz. We then selected 20 observations of 3C48 with SWIFT at times close to those for MEXART and applied the same technique to both data sets to obtain solar wind speeds. Both MEXART and SWIFT used a 50 Hz sampling rate, the frequency with which each data point is taken in the IPS time series. Additionally, we compared the resulting MFPS solar wind speeds with the STEL CCF technique. Tables 2 and 3 list dates and results from the two techniques; these tables are grouped into different time periods. Twelve pairs of the rows (24 observations) listed in Table 2 consist of simultaneous observations with two or more STEL antennas, one of which was consistently SWIFT, resulting in the ability to apply and compare both MFPS and CCF techniques within the same IPS-capable system. For May 2013 no data were analyzed with MFPS from SWIFT; therefore Table 3 only lists observations with MEXART and speeds reported from STEL.

Table 2 Determinations of solar wind speeds. First column: the system/site used; MEXART and SWIFT use the MFPS technique, and STEL uses the CCF technique. Second column: date (YYMMDD). Third column: UT time. Fourth column: heliocentric distance of the P-point in AU. Fifth column: solar wind speed ($\mathrm{km\,s^{-1}}$). Sixth column: estimated error in the determination of the speed, 1σ for the present MFPS technique, and average spread for CCF.

Technique	Date	UT	HD	V	E
STEL	090421	2.67	0.37	672	4
SWIFT	090421	2.67	0.37	630	95
MEXART	090421	18.41	0.37	690	105
SWIFT	090422	2.60	0.37	620	122
MEXART	090422	18.34	0.37	675	67
STEL	090423	2.53	0.37	643	2
SWIFT	090423	2.53	0.37	655	62
STEL	090424	2.47	0.37	627	5
SWIFT	090424	2.47	0.37	655	45
STEL	090425	2.40	0.37	625	0
SWIFT	090425	2.40	0.37	670	32
MEXART	090425	18.14	0.37	645	100
STEL	090427	2.27	0.37	557	6
STEL	090428	2.22	0.37	610	4
SWIFT	090428	2.22	0.37	625	115
STEL	120508	1.40	0.44	382	10
SWIFT	120508	1.40	0.44	380	55
MEXART	120508	17.27	0.44	415	50
STEL	120509	1.33	0.45	424	22
SWIFT	120509	1.33	0.45	430	57
MEXART	130223	22.14	0.89	350	40
SWIFT	130224	6.20	0.89	375	50
MEXART	130224	22.07	0.89	245	45
SWIFT	130225	6.13	0.89	240	12
SWIFT	130226	6.07	0.86	410	142
SWIFT	130326	4.23	0.59	385	50
SWIFT	130327	4.17	0.58	330	45
SWIFT	130328	4.10	0.57	375	32
MEXART	130328	19.98	0.56	395	80
STEL	130329	4.03	0.56	380	0
SWIFT	130329	4.03	0.56	395	57
SWIFT	130407	3.44	0.47	330	50
MEXART	130407	19.32	0.47	390	60
STEL	130408	3.38	0.46	394	4
SWIFT	130408	3.38	0.46	340	60
MEXART	130408	19.16	0.46	480	30
STEL	130409	3.31	0.44	347	37
STEL	130426	2.20	0.37	749	23
SWIFT	130426	2.20	0.37	450	65
MEXART	130426	18.08	0.37	490	80
STEL	130427	2.13	0.37	421	2
SWIFT	130427	2.13	0.37	415	77
MEXART	130427	18.00	0.37	360	85
STEL	130428	2.07	0.37	375	23
SWIFT	130428	2.07	0.37	390	50

Table 3 Determinations of speeds during May 2013. Observations with STEL CCF and MEXART MFPS techniques. Same format as Table 2.

Technique	Date	UT	HD	V	E
STEL	130522	0.50	0.57	360	17
MEXART	130522	16.37	0.57	415	72
MEXART	130523	16.30	0.58	585	22
STEL	130524	0.37	0.59	543	10
MEXART	130524	16.24	0.59	450	40
STEL	130525	0.30	0.60	476	17
MEXART	130525	16.18	0.60	595	52
STEL	130526	0.23	0.61	659	83
MEXART	130526	16.11	0.61	440	50
STEL	130527	0.17	0.62	795	60
STEL	130528	0.10	0.63	648	11
MEXART	130528	15.98	0.63	525	32
STEL	130529	0.04	0.64	593	0

4. Spectral Analysis and Model Fitting

To obtain the observed power spectra, we chose a time series of 5 120 points ($\approx$ 1 min 42 s) for MEXART and 8 192 points ($\approx$ 2 min 44 s) for SWIFT. In both cases we followed steps i) – v) below:

i) Divide the time series into subintervals of 512 points each (10.24 s), then take the fast Fourier transform and power spectra of each subinterval.
ii) Smooth the power spectra. Each point of the smoothed power spectrum becomes the average of three points: predecessor point, the point itself, and the successor point.
iii) Discard spectra with high noise at high frequencies. An integration from 2.5 Hz to 10 Hz estimates the level of noise. Spectra whose level is twice higher than the less noisy spectra are removed.
iv) Average together the remaining spectra.
v) Points at low frequencies ($<$ 0.2 Hz) of the average power spectrum are replaced by interpolated values using the line that best fits the spectrum at frequencies from 0.29 to 0.48 Hz.

The integration time (τ) used in MEXART is the time constant of an RC circuit (Manoharan, 1991; Oberoi, 2000) that obeys the system response $\mathrm{e}^{-t/\tau}$. This time provides attenuation at high spectral frequencies (f) by dividing by a factor $1 + (2\pi \tau f)^2$. This effect can be observed starting at the frequency $(2\pi\tau)^{-1}$. The SWIFT does not use a τ from an RC circuit in its receiver, this results in flat power spectra at high frequencies corresponding to white noise that has little contribution from IPS. On the other hand, the MEXART receiver power drops off at frequencies $\gtrsim$ 3 Hz (see Figure 3). We added a step for the spectrum analysis with MEXART: (v-a) to obtain a flat power at high frequencies, we divided the spectra by the off-source spectra; this way, the effect of τ is removed. Finally, for both MEXART and SWIFT: vi) the average power at high frequencies is subtracted so that only the contribution of IPS remains.

To concentrate on the region that is most involved with the solar wind speed, the Fresnel knee, we averaged neighboring points at frequencies higher than the Fresnel knee and only

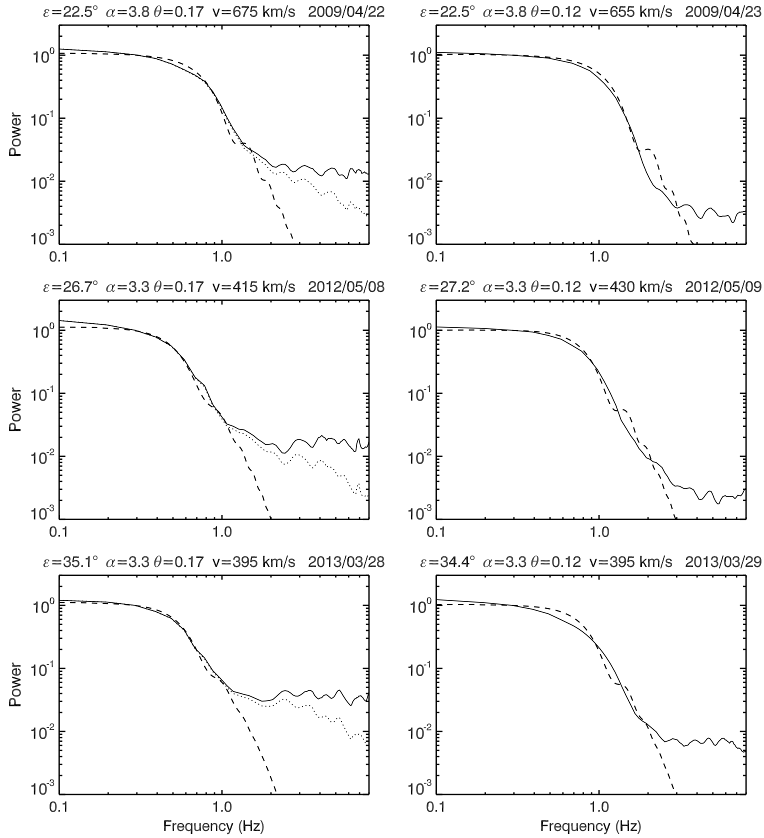

Figure 3 Examples of power spectra obtained with MEXART-140 MHz (left panels) and SWIFT-327 MHz (right panels). For MEXART, dotted and solid curves are observed spectra before and after off-source correction, respectively (before and after step (v-a) in the text). For SWIFT, solid curves are the observed spectra (no off-source correction necessary). Dashed curves are fitted theoretical spectra. Time difference between these observations is almost 8 h.

used a subset of these points, giving more weight to the part around the Fresnel knee. The power spectra at 140 and 327 MHz differ in the location of the Fresnel knee: at higher observing frequencies the knee moves to higher scintillating frequencies. For the case of the resulting power spectra with MEXART at the range of speeds of $\approx 350-650\ \mathrm{km\,s^{-1}}$, neighboring spectral points at frequencies > 0.9 Hz were averaged. An analogous average was made at frequencies > 1.3 Hz for SWIFT.

Using these fitting criteria, we found the theoretical model spectrum that best fits the spectrum obtained using this prescribed treatment. Assuming isotropic solar wind and no contribution from the inner scale, we have three free parameters left in the model: the power-law index of density turbulence spectrum α, solar wind speed $V_x(z)$, and width of the radio source θ. Then we determined these values by finding the model that minimizes the distribution

$$\chi^2 = \frac{1}{g(\alpha)} \sum_i \frac{[P_{\mathrm{O}}(f_i) - P_{\mathrm{T}}(f_i)]^2}{P_{\mathrm{O}}(f_i) P_{\mathrm{T}}(f_i)}, \tag{5}$$

where P_{O} and P_{T} represent the observed and theoretical power spectra evaluated over the range of spectral frequencies: $0.2 < f_i < 1.6$ Hz at 140 MHz and $0.2 < f_i < 1.9$ Hz at 327 MHz. A Gaussian uncertainty distribution $g(\alpha) = \exp[-(\alpha - \alpha_{\mathrm{c}})^2/0.08]$ was assumed (standard deviation = 0.2), with an expected α_{c} value depending on the epoch of solar cycle (Manoharan, Kojima, and Misawa, 1994; Glubokova, Chashei, and Tyul'bashev, 2012), $\alpha_{\mathrm{c}} = 3.8$ for solar minimum (observations of April 2009) and $\alpha_{\mathrm{c}} = 3.3$ during solar maximum (observations of 2012 and 2013). This choice of standard deviation restricts values of α that depart from α_{c}. The range explored in the fitting, for α around α_{c}, was confirmed to be large enough that it did not restrict the answers. We evaluated χ^2 for all values of the free parameters in intervals of $\Delta V_x = 5\ \mathrm{km\,s^{-1}}$, $\Delta\theta = 0.01$ and $\Delta\alpha = 0.1$. Then we obtained the values that minimize χ^2 and also tested the accuracy of the expected α.

We found the following: 1) For all the fittings α is within ± 0.1 of α_{c}. 2) The average apparent angular width θ of 3C48 at 140 and 327 MHz is 170 and 120 milliarcseconds (mas), respectively. The size at 140 MHz seems to be smaller than expected given that at 151.5 MHz Duffett-Smith and Readhead (1976) reported $\theta = 0.25 \pm 0.05$, but more IPS observations of 3C48 with MEXART are needed to verify its 140 MHz value and give an error estimate throughout the observing period. Finally, we performed a new χ^2 minimization in which we fixed $\alpha = \alpha_{\mathrm{c}}$ ($g(\alpha) = 1$), and θ to the above apparent angular widths: in this new fit, we let only $V_x(z)$ vary in intervals of $5\ \mathrm{km\,s^{-1}}$. Then the value of $V_x(z)$ minimizing this new χ^2 becomes our best value for the observed solar wind speed at the P-point. Moreover, we associated one standard deviation of uncertainty in this fitted solar wind speed by changing the speed until the resulting χ^2 distribution had become quadruple from the minimum (see *e.g.* Press *et al.*, 1986). In Figure 4 six panels corresponding to the observations carried out for the indicated six months show the calculated speeds and associated error bars. When available, observations with the multi-station technique are included. All these observations are listed in Tables 2 and 3.

5. Results of Determined Solar Wind Speeds

Figure 3 shows three examples of power spectra at 140 and 327 MHz under similar solar wind conditions. The observed spectra correspond to three near-simultaneous observations of 3C48 8 h apart in time; the estimated angular width of the radio source has been set to the average values of 170 mas at 140 MHz and 120 mas at 327 MHz. This difference in angular size produces nearly the same frequency shift between the spectra. As expected, the spectra observed with SWIFT are ≈ 1.5 shifted relative to MEXART (see Figure 2).

Figure 4 shows speeds and errors calculated three ways: single-site (MFPS) with MEXART and with SWIFT, and multi-site (CCF) with STEL. All panels, except for February 2013 and May 2013, include simultaneous observations carried out by the STEL stations. Most of the errors corresponding to these single-station results overlap the multi-station results well.

Comparing simultaneous results from SWIFT and STEL is a direct way to evaluate the accuracy of MFPS; we have twelve comparisons of this kind, which are plotted in Figure 5. These all match very well, except for one at the right hand edge, far away from the dashed line of one-to-one correspondence (on date 130426, see Table 2): this discrepancy may be related to a combination of fast and slow speeds at different positions on the LOS (*e.g.*, Moran *et al.*, 2000) or the nearby presence of a coronal mass ejection, observed previously by coronagraphs, which could abruptly have changed the assumed parameters. We leave the clarification of this particular observation for a future study. The remaining data

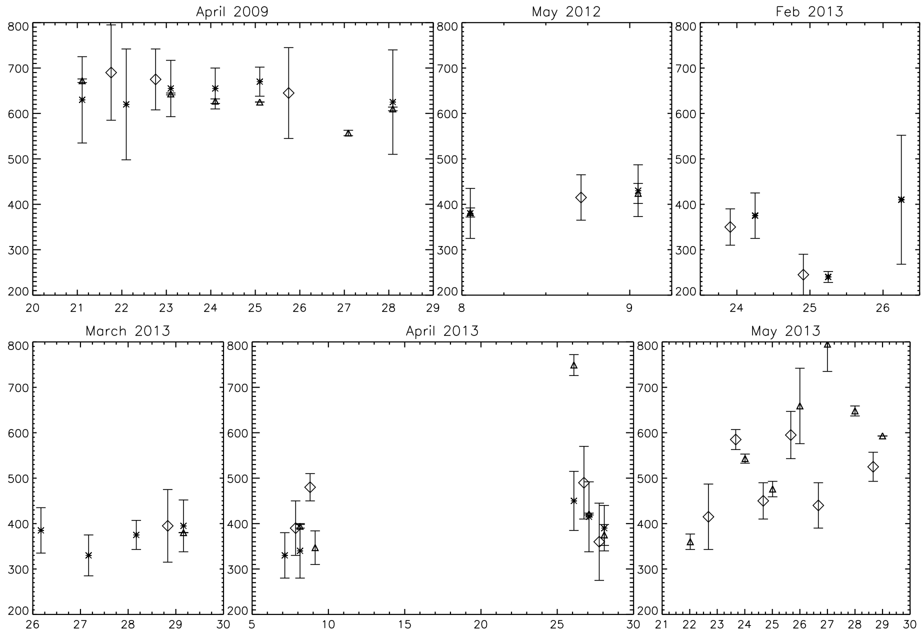

Figure 4 Solar wind speeds in vertical axes (km s^{-1}) *versus* day of month in horizontal axes. Single-station with MEXART (diamonds), single-station with SWIFT (asterisks), and multi-station with STEL (triangles).

Figure 5 Simultaneous observations with STEL and SWIFT: direct comparison between solar wind velocities using the single-station (vertical axis) and the multi-station technique (horizontal axis).

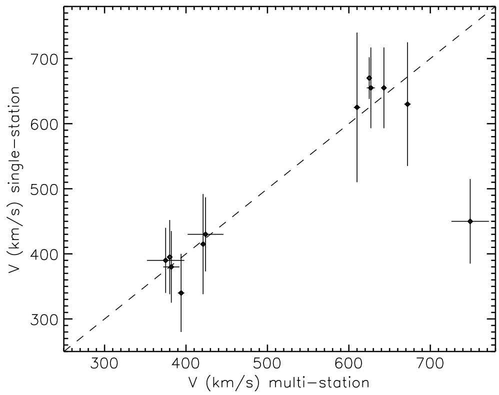

points have a correlation near to unity with no systematic tendency toward higher or lower speeds for either technique. Using STEL speeds as the true values, the average relative error of SWIFT is ≈ 4 %, while the associated fitting average error using the χ^2 distribution of Equation (5) is ≈ 14 %. Thus, MFPS results obtained with SWIFT agree with CCF results within the limits of the estimated errors for the spectral fitting.

To evaluate the accuracy for solar wind speeds obtained with MEXART, we proceeded as above with SWIFT, but here choosing a speed from 327 MHz as the true value. To compare with this, we used the speed averages measured by STEL and SWIFT (or just one of them if the other was not available), having either 8 or 16 h difference: Here the resulting average relative difference is ≈ 11 % and the fitting error ≈ 13 %. As a result of the different longitude locations, the relative difference with MEXART is expected to be larger because the true values correspond to observations carried out 8 h later or 16 h earlier. Furthermore, the change in the measured solar wind speeds observed at different locations is even stronger during periods of high activity, as can be seen in panel May 2013 of Figure 4 or Table 3. Here there are large jumps in speed (≈ 100 to $300\ \mathrm{km\,s^{-1}}$) from one day to the next, and the measurements are probably influenced by transient events.

Finally, from these solar wind results, we can compare fitted speeds between the minimum and maximum of Solar Cycle 24 in the same region of the interplanetary medium. We compared April 2009 (minimum) and April 2013 (maximum), when 3C48 appeared at 0.37 AU, around 50° to 63° in heliocentric latitude. Our average solar wind speed in this region during April 2009 was $651\ \mathrm{km\,s^{-1}}$ with a fluctuation of 4 % ($\pm 24\ \mathrm{km\,s^{-1}}$), which decreased in April 2013 to $405\ \mathrm{km\,s^{-1}}$ with a fluctuation of 14 % ($\pm 58\ \mathrm{km\,s^{-1}}$). Although these April observations correspond to a P-point location at medium-high latitudes, the LOS passes by the solar North pole during this month; the high-latitude streams can contribute to the apparent solar wind speed. This result seems to agree in general with the magnitude and fluctuations of solar wind velocities (Smith (2011) and references therein) at high latitudes that are associated with solar cycle effects, and is also consistent with the mid-latitude IPS fast solar wind reported by Bisi *et al.* (2007).

6. Summary and Conclusions

We used an MFPS technique applied to a single station to obtain remotely sensed solar wind speeds using IPS observations from both MEXART and SWIFT. Assuming isotropic solar wind turbulence, with its index α fixed depending on the solar wind epoch, a negligible contribution of the inner scale of solar wind irregularities, and constant angular width of the source 3C48 over the observational range $22° \leq \epsilon \leq 63°$, we determined the solar wind speeds that best matched the model to the observed power spectra. This way, we obtained the first solar wind speeds using MEXART IPS observations at 140 MHz. We found that the single-station solar wind speeds obtained with SWIFT using our MFPS technique agree with those from STEL using the CCF technique, and that spectra at 140 and 327 MHz have the expected relative shapes. We also provided a reliable value for the uncertainty of MFPS for the single-site speeds. Finally, the obtained speeds and their fluctuations, when the LOS crosses by the solar North pole, are as expected at these latitudes.

This survey provides an intercalibration of the single-station MFPS technique, which can now be confidently used to explore solar wind speeds. The study of the MFPS technique with observations of SWIFT is of interest because it can be applied when there are no data available from the other stations. In the future, observations using other radio sources could provide an additional test of the technique and might also yield a better understanding of the other physical parameters involved in the model of the IPS power spectrum. As the unique IPS observatory in the Americas, MEXART can complement results from other radio telescopes at different longitudes. A main goal of the MEXART project is to track solar wind disturbances in between the times of STEL and other IPS stations.

Acknowledgements The MEXART operation is funded partially by the DGAPA-PAPIIT grant IN109413 and the CONACyT grant 152471. SWIFT IPS observations were carried out under the solar wind program of the Solar-Terrestrial Environment Laboratory (STEL) of Nagoya University. We thank P. Paul Hick for a critical reading of this manuscript. We are grateful to P.K. Manoharan for his useful suggestions regarding the data analysis. J.C. Mejia-Ambriz thanks UC-MEXUS CONACyT for the postdoctoral fellowship granted to support this research. B.V. Jackson and a portion of J.C. Mejia-Ambriz's stay at UCSD has been funded by

NSF contract AGS-1053766 to the University of California, San Diego. B.V. Jackson has been supported by AFOSR contract FA9550-11-1-0324. E. Aguilar-Rodriguez acknowledges DGAPA-PAPIIT grant IN103615 and CONACyT project (grant 220981).

References

Armstrong, J.W., Coles, W.A.: 1978, Interplanetary scintillation of PSR 0531+21 at 74 MHz. *Astrophys. J.* **220**, 346. DOI.

Armstrong, J.W., Coles, W.A., Rickett, B.J.: 2000, Radio wave scattering in the outer heliosphere. *J. Geophys. Res.* **105**, 5149. DOI.

Bastian, T.S.: 2000, Propagation of radio waves in the corona and solar wind. In: Stone, R.G., Weiler, K.W., Goldstein, M.L., Bougeret, J.L. (eds.) *Radio Astronomy at Long Wavelengths*, *AGU Geophys. Monogr.* **119**, 85. DOI.

Bastian, T.S.: 2001, Radio wave propagation in the corona and the interplanetary medium. *Astrophys. Space Sci.* **277**, 107. DOI.

Bisi, M.M., Breen, A.R., Jackson, B.V., Fallows, R.A., Walsh, A.P., Mikic, Z., Riley, P., Owen, C.J., Gonzalez-Esparza, A., Aguilar-Rodriguez, E., Morgan, H., Jensen, E.A., Wood, A., Owens, M.J., Tokumaru, M., Manohara, P.K., Chashei, I.V., Giunta, A., Linker, J.A., Shishov, V.I., Tyul'bashev, S.A., Agalya, G., Glubokoba, S.K., Hamilton, M.S., Fujiki, K., Hick, P.P., Clover, J.M., Pinter, B.: 2010, From the Sun to the Earth: The 13 May 2005 coronal mass ejection. *Solar Phys.* **265**, 49. DOI.

Bisi, M.M., Fallows, R.A., Breen, A.R., Rifai Habbal, S., Jones, R.A.: 2007, Large-scale structure of the fast solar wind. *J. Geophys. Res.* **112**, A06101. DOI.

Breen, A.R., Fallows, R.A., Bisi, M.M., Jones, R.A., Jackson, B.V., Kojima, M., Dorrian, G.D., Middleton, H.R., Thomasson, P., Wannberg, G.: 2008, The solar eruption of 2005 May 13 and its effects: Long-baseline interplanetary scintillation observations of the Earth-directed coronal mass ejection. *Astrophys. J. Lett.* **683**, L79. DOI.

Breen, A.R., Fallows, R.A., Bisi, M.M., Thomasson, P., Jordan, C.A., Wannberg, G., Jones, R.A.: 2006, Extremely long baseline interplanetary scintillation measurements of solar wind velocity. *J. Geophys. Res.* **111**, A08104. DOI.

Cohen, M.H., Gundermann, E.J.: 1969, Interplanetary scintillations IV. Observations near the Sun. *Astrophys. J.* **155**, 645. DOI.

Coles, W.A., Grall, R.R., Klinglesmith, M.T., Bourgois, G.: 1995, Solar cycle changes in the level of compressive microturbulence near the Sun. *J. Geophys. Res.* **100**, 17069. DOI.

Coles, W.A., Kaufman, J.J.: 1978, Solar wind velocity estimation from multi-station IPS. *Radio Sci.* **13**, 591. DOI.

Duffett-Smith, P.J., Readhead, A.C.S.: 1976, The angular broadening of radio sources by scattering in the interstellar medium. *Mon. Not. Roy. Astron. Soc.* **174**, 7.

Fallows, R.A., Breen, A.R., Bisi, M.M., Jones, R.A., Wannberg, G.: 2006, Dual-frequency interplanetary scintillation observations of the solar wind. *Geophys. Res. Lett.* **33**, L11106. DOI.

Glubokova, S.K., Chashei, I.V., Tyul'bashev, S.A.: 2012, Small-scale solar wind density turbulence spectrum from interplanetary scintillation observations. *Adv. Astron. Space Phys.* **2**, 164.

Gonzalez-Esparza, J.A., Carrillo, A., Andrade, E., Perez-Enriquez, R., Kurtz, S.: 2004, The MEXART interplanetary scintillation array in Mexico. *Geofís. Int.* **43**, 61.

Grall, R.R., Coles, W.A., Klinglesmith, M.T., Breen, A.R., Williams, P.J.S., Markkanen, J., Esser, R.: 1996, Rapid acceleration of the polar solar wind. *Nature* **379**, 429. DOI.

Grall, R.R., Coles, W.A., Spangler, S.R., Sakurai, T., Harmon, J.K.: 1997, Observations of field-aligned density microstructure near the Sun. *J. Geophys. Res.* **102**, 263. DOI.

Hewish, A., Dennison, P.A., Pilkington, J.D.: 1966, Measurements of the size and motion of irregularities in the interplanetary medium. *Nature* **209**, 1188. DOI.

Hewish, A., Scott, P.F., Wills, D.: 1964, Interplanetary scintillation of small diameter radio sources. *Nature* **203**, 1214. DOI.

Jackson, B.V., Clover, J.M., Hick, P.P., Buffington, A., Bisi, M.M., Tokumaru, M.: 2013, Inclusion of real-time in-situ measurements into the UCSD time-dependent tomography and its use as a forecast algorithm. *Solar Phys.* **285**, 151. DOI.

Jackson, B.V., Hick, P.L., Kojima, M., Yokobe, A.: 1998, Heliospheric tomography using interplanetary scintillation observations 1. Combined Nagoya and Cambridge data. *J. Geophys. Res.* **103**, 12049. DOI.

Jackson, B.V., Hick, P.P., Bisi, M.M., Clover, J.M., Buffington, A.: 2010, Inclusion of in-situ velocity measurements into the UCSD time-dependent tomography to constrain and better-forecast remote-sensing observations. *Solar Phys.* **265**, 245. DOI.

Janardhan, P., Alurkar, S.K.: 1993, Angular source size measurements and interstellar scattering at 103 MHz using interplanetary scintillation. *Astron. Astrophys.* **269**, 119.
Kojima, M., Coles, W.A., Tokumaru, M., Fujiki, K.: 2013, Scintillation measurements of the solar wind velocity in strong scattering near the Sun. *Solar Phys.* **283**, 519. DOI.
Kojima, M., Tokumaru, M., Watanabe, H., Yokobe, A., Asai, K., Jackson, B.V., Hick, P.L.: 1998, Heliospheric tomography using interplanetary scintillation observations II. Latitude and heliocentric distance dependence of solar wind structure at 0.1 – 1 AU. *J. Geophys. Res.* **103**, 1981. DOI.
Little, L.T., Hewish, A.: 1966, Interplanetary scintillaton and its relation to the angular structure of radio sources. *Mon. Not. Roy. Astron. Soc.* **134**, 221.
Manoharan, P.K.: 1991, Study of the solar wind using single-station interplanetary scintillation. Ph.D. thesis, University of Bombay.
Manoharan, P.K.: 2010, Ooty interplanetary scintillation – Remote-sensing observations and analysis of coronal mass ejections in the Heliosphere. *Solar Phys.* **265**, 137. DOI.
Manoharan, P.K., Ananthakrishnan, S.: 1990, Determination of solar-wind velocities using single-station measurements of interplanetary scintillation. *Mon. Not. Roy. Astron. Soc.* **244**, 691.
Manoharan, P.K., Kojima, M., Misawa, H.: 1994, The spectrum of electron density fluctuations in the solar wind and its variations with solar wind speed. *J. Geophys. Res.* **99**, 23411. DOI.
Mejia-Ambriz, J.C., Villanueva-Hernandez, P., Gonzalez-Esparza, J.A., Aguilar-Rodriguez, E., Jeyakumar, S.: 2010, Observations of interplanetary scintillation (IPS) using the Mexican Array Radio Telescope (MEXART). *Solar Phys.* **265**, 209. DOI.
Moran, P.J., Ananthakrishnan, S., Balasubramanian, V., Breen, A.R., Canals, A., Fallows, R.A., Janardhan, P., Tokumaru, M., Williams, P.J.S.: 2000, Observations of interplanetary scintillation during the 1998 whole Sun month: A comparison between EISCAT, ORT and Nagoya data. *Ann. Geophys.* **18**, 1003. DOI.
Oberoi, D.: 2000, Tomography of the solar wind using interplanetary scintillation. Ph.D. thesis, Indian Institute of Science.
Press, W., Flannery, B., Teukolsky, S., Vetterling, W.: 1986, *Numerical Recipes*, Cambridge University Press, New York, 535.
Rao, A.P., Ananthakrishnan, S., Balasubramanian, V., Oberoi, D., Coles, W.A.: 1996, Very long baseline IPS observations of the solar wind speed in the fast polar streams. In: Winterhalter, D., Gosling, J.T., Habbal, S.R., Kurth, W.S., Neugebauer, M. (eds.) *Proceedings of the Eighth International Solar Wind Conference*, *AIP Conf. Proc.* **382**, 511. DOI.
Readhead, A.C.S.: 1971, Interplanetary scintillation of radio sources at metre wavelengths II. Theory. *Mon. Not. Roy. Astron. Soc.* **155**, 185.
Readhead, A.C.S., Kemp, M.C., Hewish, A.: 1978, The spectrum of small-scale density fluctuations in the solar wind. *Mon. Not. Roy. Astron. Soc.* **185**, 207.
Rickett, B.J., Coles, W.A.: 2000, Scattering in the solar wind at long wavelengths. In: Stone, R.G., Weiler, K.W., Goldstein, M.L., Bougeret, J.L. (eds.) *Radio Astronomy at Long Wavelengths*, *AGU Geophys. Monogr.* **119**, 97. DOI.
Salpeter, E.E.: 1967, Interplanetary scintillations. I. Theory. *Astrophys. J.* **147**, 433. DOI.
Scott, S.L., Coles, W.A., Bourgois, G.: 1983, Solar wind observations near the Sun using interplanetary scintillation. *Astron. Astrophys.* **123**, 207.
Scott, S.L., Rickett, B.J., Armstrong, J.W.: 1983, The velocity and the density spectrum of the solar wind from simultaneous three-frequency IPS observations. *Astron. Astrophys.* **123**, 191.
Shen, Z.Q., Lo, K.Y., Liang, M.C., Ho, P.T.P., Zhao, J.H.: 2005, A size of 1 AU for the radio source Sgr A* at the centre of the Milky Way. *Nature* **438**, 62. DOI.
Smith, E.J.: 2011, Solar cycle evolution of the heliospheric magnetic field: The Ulysses legacy. *J. Atmos. Solar-Terr. Phys.* **73**, 277. DOI.
Swarup, G., Sarma, N.V.G., Joshi, M.N., Kapahi, V.K., Bagri, D.S., Damle, S.H., Ananthakrishnan, S., Balasubramanian, V., Bhave, S.S., Sinha, R.P.: 1971, Large steerable radio telescope at Ootacamund, India. *Nature* **230**, 185. DOI.
Tappin, S.J., Howard, T.A.: 2010, Reconstruction CME structures from IPS observations using a phenomenological model. *Solar Phys.* **265**, 159. DOI.
Tokumaru, M., Kojima, M., Fujiki, K., Maruyama, K., Maruyama, Y., Ito, H., Iju, T.: 2011, A newly developed UHF radiotelescope for interplanetary scintillation observations: Solar wind imaging facility. *Radio Sci.* **46**, RS0F02. DOI.
Vitkevich, T., Vlasov, V.I.: 1970, Radioastronomical investigations of the drift of the inhomogeneous interplanetary plasma. *Soviet Astron.* **13**, 669.
Yamauchi, Y., Kojima, M., Tokumaru, M., Misawa, H., Morl, H., Tanaka, T., Takaba, H., Kondo, T., Manoharan, P.K.: 1996, Micro-turbulence in the solar wind at 5 – 76 Rs observed with interplanetary scintillation. *J. Geomagn. Geoelectr.* **48**, 1201. DOI.